Noname manuscript No.
(will be inserted by the editor)

High-performance Parallel Solver for Integral Equations of Electromagnetics Based on Galerkin Method

Mikhail Kruglyakov · **Lidia Bloshanskaya**

Received: / Accepted:

Abstract A new parallel solver for the volumetric integral equations (IE) of electrodynamics is presented. The solver is based on the Galerkin method which ensures the convergent numerical solution. The main features include: (i) the memory usage is 8 times lower, compared to analogous IE based algorithms, without additional restriction on the background media; (ii) accurate and stable method to compute matrix coefficients corresponding to the IE; (iii) high degree of parallelism. The solver's computational efficiency is shown on a problem of magnetotelluric sounding of the high conductivity contrast media. A good agreement with the results obtained with the second order finite element method is demonstrated. Due to effective approach to parallelization and distributed data storage the program exhibits perfect scalability on different hardware platforms.

Keywords Integral equations · Forward modeling · Electromagnetic sounding · Galerkin method · Green's tensor · High-performance computing

1 Introduction

Electromagnetic (EM) methods of geophysics are used to model the subsurface electrical conductivity distribution. Conductivity is affected by the rock type and composition, temperature, and fluid/melt content and thus can be used in various engineering and industrial problems like detecting hydrocarbon (low-conductive) and

Mikhail Kruglyakov (✉)
Faculty of Computational Mathematics and Cybernetics, Lomonosov MSU, GSP-1,
Leninskiye Gory, 1-52, 119991 Moscow, Russia
Tel. +74959391919 Fax. +74959392596
Institute of Geophysics, ETH Zurich, Sonneggstrasse 5, 8092 Zurich, Switzerland
E-mail: mkruglyakov@cs.msu.su

Lidia Bloshanskaya
SUNY New Paltz, Department of Mathematics, 1 Hawk Dr, New Paltz, NY 12561, U.S.A.
E-mail: bloshanl@newpaltz.edu

geothermal or ore (high-conductive) reservoirs. Measured electrical and/or magnetic fields are further interpreted via the calculations for a given three-dimensional model of conductivity distribution. Maxwell's equation describing the EM field distribution can not be solved analytically in general case requiring numerical simulation. Large number of such simulations is required, and complex large scale models are invoked, Chave and Jones (2012).

The growing amount of data calls for the development of new numerical methods capable to deliver fast and accurate EM simulations and harness the computational power provided by modern high-performance multi-core and multi-node platforms.

There are three basic approaches to the numerical simulation of EM fields in the conductive media: finite-difference (FD), finite-element (FE) and volumetric integral equation (IE) methods. The FD schemes dominated in EM sounding for decades, Mackie et al (1994); Haber and Ascher (2001); Newman and Alumbaugh (2002); Egbert and Kelbert (2012); Jaysaval et al (2015). However, the FE methods has become popular in recent years, Schwarzbach et al (2011); Farquharson and Miensopust (2011); Puzyrev et al (2013); Ren et al (2013); Grayver and Kolev (2015). The IE methods are not so common due to the certain difficulties in their implementation. For their usage one can refer to Avdeev et al (2002); Hursan and Zhdanov (2002); Singer (2008); Koyama et al (2008); Kamm and Pedersen (2014).

The main difference in these approaches is in the discretization outcome. The model usually consists of a number of the non uniform three-dimensional anomalies embedded in the one-dimensional (layered) background media. While the FD and FE methods produce large sparse systems, Ernst and Gander (2012), the IE method results in the compact dense system matrices. The compactness is attained since the modeling region is confined only to the three-dimensional conductivity structures (anomalies) under the investigation, Raiche (1974); Weidelt (1975). Note that boundary conditions are satisfied by construction of the Green's functions. By contrast, in the FD and FE methods one has to discretize a volume much bigger in both lateral and vertical directions in order to enable the decay (or stabilization) of the EM field at the boundaries of the modeling domain, Grayver and Kolev (2015); Mulder (2006). Another distinction between the methods is in the condition number of matrices (it controls the stability of the solution). In FD and FE methods the condition number depends on the discretization and frequency, whereas in IE approach it does not, Pankratov et al (1995); Singer (1995).

The main focus in development and implementation of the numerical methods for the IE is the efficiency and performance for the large number of unknown parameters. The proposed new iterative numerical solver for the IE addresses this issue both mathematically (increasing the accuracy and stability of coefficient computations and reducing the memory usage) and computationally (allowing high degree of parallelism without memory loss at the nodes). The special class of integral equations is used: the integral equations with contracting kernel (CIE), Pankratov et al (1995); Singer (1995). The CIE were proved to have a unique solution and a well-conditioned (by construction) system matrix, Pankratov et al (1995); Singer (1995). The Galerkin method is used to solve CIE numerically, Delves and Mohamed (1985). In Kruglyakov (2011); Singer (2008) it was proved that the corresponding solution converges.

Two main issues in the IE numerical solution are the calculation of matrix coefficients with sufficient accuracy, Wannmaker (1991), and the storage of this dense matrix in some packed form, Avdeev et al (1997, 2002). The Galerkin method with piece-wise constant basis allows to address both of these issues. Namely, the system matrix is decomposed into sums and products of diagonal and block-Toeplitz matrices. First, matrix coefficients (i.e., double volumetric integrals of the product of basis functions and CIE kernel) are analytically transformed into the one-dimensional convolution integrals. These convolution integrals are then computed by digital filtering approach. Keep in mind, that only weights of these filters are computed numerically, whereas the functions in the knots are computed analytically. The resulting system is solved using the Flexible GMRES, Saad (1993).

The proposed solver exhibits three main features. 1) The memory usage is 8 times lower, compared to the analogous IE solving algorithms. It is important to stress that the memory is saved for any background with an arbitrary number of layers. In contrast, in Kamm and Pedersen (2014) the memory reduction is achieved only in case of homogenous half-space as a background and for uniform vertical discretization. In Avdeev and Knizhnik (2009); Koyama et al (2008); Sun and Kuvshinov (2015) it is achieved at the expense of accuracy and performance. The idea behind the proposed solver is to combine the Galerkin method with the properties of EM field, namely Lorentz reciprocity. The matrix of the ensuing linear system can be separated in symmetric and antisymmetric submatricies. This reduces the memory requirements by 8 times, Sect. 3. 2) Efficient and accurate method for the computation of these matrices, Sect. 3. 3) The implementation with high degree of parallelism. The computational experiments performed with "Bluegene" and "Lomonosov" supercomputers from MSU, and high-performance computer (HPC) "Piz Daint" from Swiss National Supercomputing Center show that the solver makes the best usage of 128 to 2,048 nodes for calculation at a single frequency and a single source. The program exhibits perfect scalability.

This paper is organized as follows. Section 2 is devoted to the overview of the CIE approach and the construction of the approximating system of linear equations. Section 3 addresses the reduction in memory requirements, the computation of matrix coefficients, and features of parallel implementation. In Sect. 4 the computational results for high (more than $3 \cdot 10^4$) conductivity contrast COMMEMI3D-3 model (Hursan and Zhdanov (2002); Varentsov et al (2000)) are compared with the corresponding results obtained using FE method by Grayver and Kolev (2015). The Appendices A to C provide the mathematical details of the presented method.

2 Contracting Integral Equation

2.1 Overview

Assume that the EM fields are induced by the external electric currents $\mathbf{J}_{ext}$. Moreover, assume that the EM fields are time dependent as $e^{-i\omega t}$, where ω is an angular frequency, $i = \sqrt{-1}$ and magnetic permeability μ_0 is the same in whole space. Let $\sigma(M)$, $\mathbf{Re}\,\sigma(M) \geq 0$ be a three-dimensional complex conductivity distribution in

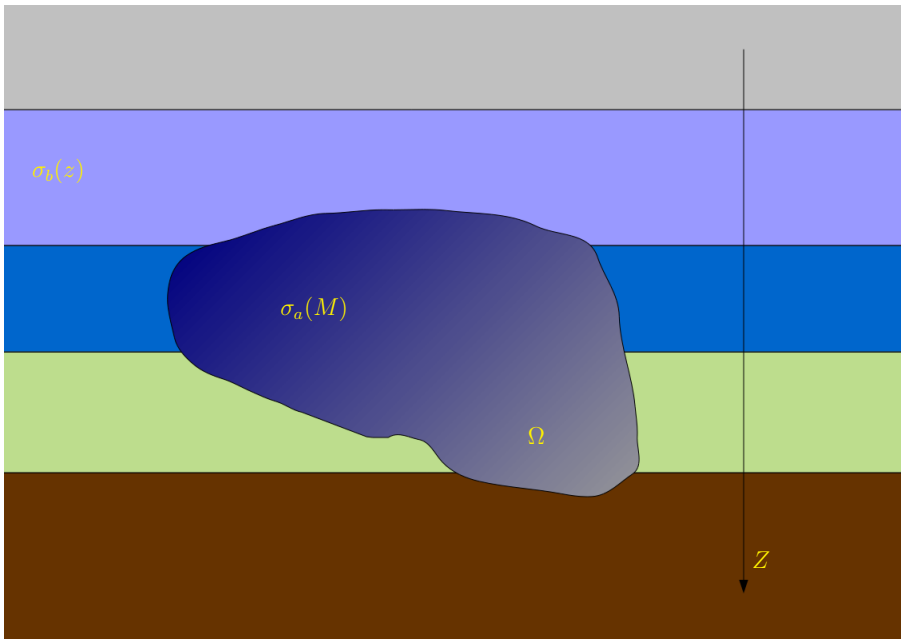

Fig. 1: Typical model

space. Then the electrical field $\mathbf{E}$ and the magnetic field $\mathbf{H}$ give the solution of the system of Maxwell's equations

$$\begin{cases} \operatorname{curl}\mathbf{H} = \sigma\mathbf{E} + \mathbf{J}_{ext}, \\ \operatorname{curl}\mathbf{E} = i\omega\mu_0\mathbf{H}. \end{cases} \tag{1}$$

The solution of (1) is unique under the additional radiation conditions at infinity, Ward and Hohmann (1988).

Let $\Omega \subset \mathbf{R}^3$ be some bounded domain and $\sigma(M) = \sigma_b(z)$ for $M(x,y,z) \notin \Omega$ and $\sigma(M) = \sigma_a(M)$ for $M \in \Omega$ (Fig. 1). Then for any $M \in \mathbf{R}^3$ the fields $\mathbf{E}(M)$ and $\mathbf{H}(M)$ are expressed in terms of the integrals

$$\begin{aligned} \mathbf{E}(M) &= \mathbf{E}^N(M) + \int\limits_{\Omega} \widehat{G}^E(M,M_0)\,(\sigma_a(M_0) - \sigma_b(M_0))\,\mathbf{E}(M_0)d\Omega_{M_0}, \\ \mathbf{H}(M) &= \mathbf{H}^N(M) + \int\limits_{\Omega} \widehat{G}^H(M,M_0)\,(\sigma_a(M_0) - \sigma_b(M_0))\,\mathbf{E}(M_0)d\Omega_{M_0}. \end{aligned} \tag{2}$$

Here $\widehat{G}^E$, $\widehat{G}^H$ are electrical and magnetic Green's tensors respectively, Dmitriev et al (2002); Pankratov et al (1995). The terms $\mathbf{E}^N$, $\mathbf{H}^N$ are called the normal electric and magnetic fields, corresponding. They form the solution of the system

$$\begin{cases} \operatorname{curl}\mathbf{H}^N = \sigma_b(z)\mathbf{E}^N + \mathbf{J}_{ext}, \\ \operatorname{curl}\mathbf{E}^N = i\omega\mu_0\mathbf{H}^N \end{cases} \tag{3}$$

with corresponding conditions at the infinity. Note, that $\widehat{G}^E$, $\widehat{G}^H$ are indepent of the anomalous conductivity σ_a.

Let $\mathbf{L}_2[\Omega]$ be a Hilbert functional space of vector functions $\mathbf{V}$ with the following norm and dot product

$$\begin{aligned}(\mathbf{V},\mathbf{U})_{\mathbf{L}_2[\Omega]} &= \int\limits_{\Omega} \left(V_x(M)\overline{U}_x(M)+V_y(M)\overline{U}_y(M)+V_z(M)\overline{U}_z(M)\right) d\Omega_M,\\ \|\mathbf{V}\|_{\mathbf{L}_2[\Omega]} &= \sqrt{(\mathbf{V},\mathbf{V})}.\end{aligned} \tag{4}$$

Suppose $\mathbf{Re}\,\sigma_b(z) > 0$ for $M(x,y,z) \in \Omega$ (the typical EM sounding situation), then the operator $\mathbf{G}_{\mathrm{E}}^{\mathrm{m}}$ is defined as

$$\mathbf{G}_{\mathrm{E}}^{\mathrm{m}}\mathbf{V} = \sqrt{\mathbf{Re}\,\sigma_b}\,\widehat{\mathrm{G}}^{\mathrm{E}}\left[2\sqrt{\mathbf{Re}\,\sigma_b}\mathbf{V}\right] + \mathbf{V}, \tag{5}$$

where $\widehat{\mathrm{G}}^{\mathrm{E}}$ is an integral operator from the first equation in (2). The operator $\mathbf{G}_{\mathrm{E}}^{\mathrm{m}}$ is a contracting operator in $\mathbf{L}_2[\Omega]$, Pankratov et al (1995); Singer (1995). Using (2) and (5) one obtains the CIE for $\mathbf{E}$

$$\begin{aligned}&\left(\mathrm{I}-\mathbf{G}_{\mathrm{E}}^{\mathrm{m}}\frac{b}{a}\right)\widetilde{\mathbf{E}} = \sqrt{\mathbf{Re}\,\sigma_b}\mathbf{E}^N,\\ &\widetilde{\mathbf{E}} = a\mathbf{E}, \quad a = \frac{\sigma_a+\overline{\sigma_b}}{2\sqrt{\mathbf{Re}\,\sigma_b}} \quad b = \frac{\sigma_a-\sigma_b}{2\sqrt{\mathbf{Re}\,\sigma_b}},\end{aligned} \tag{6}$$

where I is the identity operator and $\overline{\sigma_b}$ means complex conjugation of σ_b.

2.2 Galerkin Method

Suppose the domain Ω is divided in nonoverlapping subdomains $\Omega = \cup\Omega_n$, $n = 1\ldots N$ and $\sigma_b(M) = \sigma_b^n$, $\sigma_a(M) = \sigma_a^n$ for $M \in \Omega_n, n = 1\ldots N$. For each subdomain Ω_n define the function $W_n(M)$ as

$$W_n(M) = \begin{cases}\dfrac{1}{V_n}, & M \in \Omega_n,\\ 0, & M \notin \Omega_n,\end{cases} \quad V_n = \int\limits_{\Omega_n} d\Omega_M, \quad n = 1\ldots N. \tag{7}$$

Let $\widetilde{\mathbf{W}}^N$ be a linear span of the vector functions $\mathbf{W}_n$, $\mathbf{W}_n = (W_{n_x}, W_{n_y}, W_{n_z})$, $n_x, n_y, n_z = 1\ldots N$ and $\mathbf{P}^{\mathrm{N}}$ be a projection operator from $\mathbf{L}_2[\Omega]$ to $\widetilde{\mathbf{W}}^N$

$$\forall \mathbf{F} \in \mathbf{L}_2[\Omega] \quad \left[\mathbf{P}^{\mathrm{N}}[\mathbf{F}]\right]_\gamma = \sum_{n=1}^{N} \alpha_n^\gamma W_n, \quad \alpha_n^\gamma = \frac{\int\limits_{\Omega_n} F_\gamma(M) d\Omega_M}{V_n}, \tag{8}$$

where $\gamma = x,y,z$. Note that $\left\|\mathbf{P}^{\mathrm{N}}\right\| = 1$.

Applying $\mathbf{P}^{\mathrm{N}}$ to the first equation in (6) one obtains the operator equation in $\widetilde{\mathbf{W}}^N$

$$\begin{aligned}&\mathbf{W} - \mathbf{P}^{\mathrm{N}}\mathbf{G}_{\mathrm{E}}^{\mathrm{m}}\frac{b}{a}\mathbf{W} = \mathbf{W}^0,\\ &\mathbf{W}^0 = \mathbf{P}^{\mathrm{N}}\sqrt{\mathbf{Re}\,\sigma_b}\mathbf{E}^N.\end{aligned} \tag{9}$$

Since $\frac{b}{a} < 1$, $\mathbf{G}_{\mathrm{E}}^{\mathrm{m}}$ is a contracting operator and $\left\|\mathbf{P}^{\mathrm{N}}\right\| = 1$, it can be easily shown that (9) has a unique solution $\mathbf{W}$ in $\widetilde{\mathbf{W}}^N$, Kruglyakov (2011); Singer (2008). Moreover, $\mathbf{W}$ approximates $\mathbf{E}$ with the first order of d in $\mathbf{L}_2[\Omega]$, where $d = \max\limits_{n=1\ldots N} d_n$, d_n is a diameter of the subdomain Ω_n, Kruglyakov (2011).

Using the definition of $\widetilde{\mathbf{W}}^N$ the components of $\mathbf{W} = (W_x, W_y, W_z)$ can be expressed as

$$W_\gamma = \sum_{k=1}^{N} U_n^\gamma W_n, \quad \gamma = x, y, z. \tag{10}$$

Using (8) to (10) and taking into account that σ_a, σ_b are piecewise functions, one obtains the following system of linear equations for the coefficients $\mathbf{U}_n = (U_n^x, U_n^y, U_n^z)$, $n = 1 \ldots N$

$$\mathbf{U}_n - \sum_{m=1}^{N} \hat{\gamma}^m \widehat{K}_n^m \mathbf{U}_m = \mathbf{U}_n^0, \tag{11}$$

where

$$\begin{aligned}
\widehat{K}_n^m &= \hat{I} + \frac{2}{V_n} \sqrt{\mathbf{Re}\, \sigma_b^m \, \mathbf{Re}\, \sigma_b^n} \hat{B}_n^m, \\
\widehat{B}_n^m &= \int\limits_{\Omega_n} \int\limits_{\Omega_m} \widehat{G}^E(M, M_0) d\Omega_{M_0} d\Omega_M, \\
\hat{\gamma}^m &= \frac{\sigma_a^m - \sigma_b^m}{\sigma_a^m + \overline{\sigma_b^m}}, \\
\mathbf{U}_n^0 &= \frac{\sqrt{\mathbf{Re}\, \sigma_b^n}}{V_n} \int\limits_{\Omega_n} \mathbf{E}^N(M) d\Omega_M.
\end{aligned} \tag{12}$$

Note that $\widehat{K}_n^m$, $\widehat{B}_n^m$, $\hat{I}$, $\hat{\gamma}^m$ are 3×3 matrices, $\hat{I}$ is an identity matrix, $\hat{\gamma}^m$ is a diagonal matrix. The system (11) has a unique solution, Kruglyakov (2011); Singer (2008).

Using the solution $\mathbf{U}_n$ of system (11) one can approximate $\widetilde{\mathbf{E}}(M)$ and $\widetilde{\mathbf{H}}(M)$ for any point $M \in R^3$ with

$$\begin{aligned}
\mathbf{E}(M) \approx \widetilde{\mathbf{E}}(M) &= \mathbf{E}^N(M) + \sum_{n=1}^{N} (\sigma_a^n - \sigma_b^n) \mathbf{U}_n \int\limits_{\Omega_n} \widehat{G}^E(M, M_0) d\Omega_{M_0}, \\
\mathbf{H}(M) \approx \widetilde{\mathbf{H}}(M) &= \mathbf{E}^H(M) + \sum_{n=1}^{N} (\sigma_a^n - \sigma_b^n) \mathbf{U}_n \int\limits_{\Omega_n} \widehat{G}^H(M, M_0) d\Omega_{M_0}.
\end{aligned} \tag{13}$$

Relations (13) are first order approximations of d in $\mathbf{C}$ for $M \notin \Omega$, Kruglyakov (2011), and result in fast and relatively simple computations. The main challenge is to calculate matrix coefficients and solve the system (11).

3 Computational Challenges

3.1 Memory Requirements

The main challenge of the integral equation approach is in solving of the system of linear equations with dense matrices (11). The storage of these matrices in RAM is also problematic. The standard approach, Avdeev et al (1997), is to use the property

$$\widehat{G}^E(M,M_0) = \widehat{G}^E(x-x_0, y-y_0, z, z_0). \tag{14}$$

For the implementation purposes consider now $\Omega \subset R^3$ to be a rectangular domain. As before Ω is divided in $N = N_x N_y N_z$ rectangular subdomains Ω_n, $n = 1,\ldots,N$, where N_x, N_y, N_z are the number of subdomains in X, Y, Z directions respectively. Suppose also that each Ω_n has the same size $h_x \times h_y$ in XY plane. Then

$$\widehat{B}_n^m = \int\limits_{\Omega_n}\int\limits_{\Omega_m} \widehat{G}^E(M,M_0) d\Omega_{M_0} d\Omega_M = \widehat{B}_n^m \left(I_x^n - I_x^m, I_y^n - I_y^m, I_z^n, I_z^m\right), \tag{15}$$

where $I_x^n, I_x^m \in \{1,2,\ldots N_x\}$, $I_y^n, I_y^m \in \{1,2,\ldots N_y\}$, $I_z^n, I_z^m \in \{1,2,\ldots N_z\}$, $n,m = 1\ldots N$. Therefore $\widehat{B}_n^m$ is a block Toeplitz matrix induced by the block vector $(C^y_{-(N_y-1)}$, $C^y_{-(N_y-2)}, \ldots, C^y_{N_y-2}, C^y_{N_y-1})$. Each block C_i^y, $i = -(N_y-1)\ldots N_y-1$ is also a block Toeplitz matrix and is induced by the block vector $(D^i_{-(N_x-1)}, D^i_{-(N_x-2)}, \ldots D^i_{N_x-2}, D^i_{N_x-1})$. The D_j^i is a 3×3 block matrix with the structure

$$D_j^i = Q(i,j) = \begin{pmatrix} Q_{xx} & Q_{xy} & Q_{xz} \\ Q_{yx} & Q_{yy} & Q_{yz} \\ Q_{zx} & Q_{zy} & Q_{zz} \end{pmatrix}. \tag{16}$$

Here $Q_{\alpha\beta}$ are the matrices of the order N_z, $\alpha,\beta = x,y,z$, $i = -(N_y-1)\ldots N_y-1$, $j = -(N_x-1)\ldots N_x-1$.

Let A be a matrix corresponding to the system of linear equations (11). Then

$$A = S + R_1 B R_2, \tag{17}$$

where S, R_1, R_2 are the diagonal matrices; $B = \left\{\widehat{B}_n^m\right\}$ is the block Toeplitz matrix described above.

In view of (17) it follows that only $36 \cdot N_x N_y N_z^2 \cdot 16 + O(N_x N_y N_z)$ bytes are required to store matrix A in double precision. Using the equivalence $G^E_{xy} = G^E_{yx}$ this requirement can be reduced to $32 \cdot N_x N_y N_z^2 \cdot 16 + O(N_x N_y N_z)$ bytes as in Avdeev et al (1997). This memory requirement can be reduced in 8 times by virtue of the following Lemmas.

Lemma 1 *If $\widehat{G}^E(M,M_0)$ is an electrical Green's tensor of any layered media, then it possesses symmetric and antisymmetric properties in Cartesian coordinates along*

the vertical dimension

$$
\begin{aligned}
G^E_{xx}(x-x_0,y-y_0,z,z_0) &= G^E_{xx}(x-x_0,y-y_0,z_0,z),\\
G^E_{yy}(x-x_0,y-y_0,z,z_0) &= G^E_{yy}(x-x_0,y-y_0,z_0,z),\\
G^E_{zz}(x-x_0,y-y_0,z,z_0) &= G^E_{zz}(x-x_0,y-y_0,z_0,z),\\
G^E_{xy}(x-x_0,y-y_0,z,z_0) &= G^E_{yx}(x-x_0,y-y_0,z,z_0),\\
G^E_{xy}(x-x_0,y-y_0,z,z_0) &= G^E_{xy}(x-x_0,y-y_0,z_0,z),\\
G^E_{zx}(x-x_0,y-y_0,z,z_0) &= -G^E_{xz}(x-x_0,y-y_0,z_0,z),\\
G^E_{zy}(x-x_0,y-y_0,z,z_0) &= -G^E_{yz}(x-x_0,y-y_0,z_0,z).
\end{aligned}
\tag{18}
$$

Lemma 2 *If $\widehat{G}^E(M,M_0)$ is an electrical Green's tensor of any layered media, then it possesses symmetric and antisymmetric properties in Cartesian coordinates along the lateral dimensions*

$$
\begin{aligned}
G^E_{\alpha\alpha}(x-x_0,y-y_0,z,z_0) &= G^E_{\alpha\alpha}(x_0-x,y-y_0,z,z_0) =\\
G^E_{\alpha\alpha}(x-x_0,y_0-y,z,z_0) &= G^E_{\alpha\alpha}(x_0-x,y_0-y,z,z_0),\\
G^E_{xy}(x-x_0,y-y_0,z,z_0) &= -G^E_{xy}(x_0-x,y-y_0,z,z_0) =\\
-G^E_{xy}(x-x_0,y_0-y,z,z_0) &= G^E_{xy}(x_0-x,y_0-y,z,z_0),\\
G^E_{zx}(x-x_0,y-y_0,z,z_0) &= -G^E_{zx}(x_0-x,y-y_0,z,z_0) =\\
G^E_{zx}(x-x_0,y_0-y,z,z_0) &= -G^E_{zx}(x_0-x,y_0-y,z,z_0),\\
G^E_{zy}(x-x_0,y-y_0,z,z_0) &= G^E_{zy}(x_0-x,y-y_0,z,z_0) =\\
-G^E_{zy}(x-x_0,y_0-y,z,z_0) &= -G^E_{zy}(x_0-x,y_0-y,z,z_0),\\
\alpha &\in \{x,y,z\}.
\end{aligned}
\tag{19}
$$

These Lemmas are trivial corollaries from Lorentz reciprocity, Ward and Hohmann (1988) and formulas for the Green's tensor components (See Appendix A). Relations (15) and (18) give

$$
\begin{aligned}
&Q_{zx} = -Q^T_{xz}, Q_{zy} = -Q^T_{yz},\\
&Q_{xx} = Q^T_{xx}, Q_{yy} = Q^T_{yy}, Q_{zz} = Q^T_{zz},\\
&Q_{xy} = Q^T_{xy} = Q_{yx} = Q^T_{yx},
\end{aligned}
\tag{20}
$$

where ^{T} indicates a matrix transpose.

Therefore, one needs to store only Q_{xz}, Q_{yz} and upper diagonal parts of Q_{xx}, Q_{xy}, Q_{yy}, Q_{zz}. Moreover the values $Q(i,j)$ can be stored only for $i = 0,\dots,N_y-1, j = 0,\dots,N_x-1$, since (19) allows to obtain these values for negative i or j from suitable symmetric/antisymmetric properties.

Thus only $2\cdot N_xN_yN_z\cdot(2N_z+1)\cdot 16$ bytes are required to store $\widehat{B}^m_n$ which is 8 times less than the memory requirements in Avdeev et al (1997, 2002); Hursan and Zhdanov (2002). It is worth to stress again, that this is valid for any background layered media and without the conditions on the subdomains to be of the same vertical sizes.

3.2 Matrix Coefficients Computation

The next computational challenge of the Galerkin approach is the evaluation of the coefficients $\widehat{B}_n^m$, $n,m = 1\ldots N$, that is the double volumetric integrals of the $\widehat{G}^E$ in the RHS of (15), with desired accuracy. The components of $\widehat{G}^E$ are the improper integrals containing the Bessel functions, Appendix A. The integration in vertical direction is performed analytically using the fundamental function of layered media approach from Dmitriev et al (2002), Appendix B. The main problem, however, is the integration over the horizontal domains. In this case one needs to compute the fifth-order integrals over the fast-oscillating functions.

The integrals in (15) are double volumetric ones, thus they have only weak singularity. Therefore, one can change the order of integration and make an appropriate substitution and convert the fifth-order integral to a convolution with the specific kernel. Following the standard approach of convolution calculation the spectrum of this kernel is computed and the digital filter is constructed, Appendix C.

It is important to emphasize that both the knots and the weights in the obtained filter significantly depend on the integration domains. On the contrary, the integration over different horizontal domains is completely data independent. This is used in parallel algorithm. The computational experiments demonstrate (Sect. 4) that the used filters provide suitable accuracy even for the models with high conductivity contrast.

3.3 Parallel Implementation

The most essential part of any iterative method for solving a system of linear equations is the matrix-vector multiplication. Since matrix B is a block Toeplitz matrix, one can use the two-dimensional Fast Fourier Transform (FFT) to speed up this operation, Avdeev et al (1997). Therefore, instead of matrices $Q(i,j)$ the discrete Fourier transformations $\widetilde{Q}(i,j)$ are stored. This requires the same amount of memory since the discrete Fourier transform preserves the symmetric/antisymmetric properties of data.

The multiplication of block Toeplitz matrix B on some vector $\mathbf{V} \in \widetilde{\mathbf{W}}^N$ is performed via the following three-step algorithm:

1. Compute $3N_z$ forward FFT of vector $\mathbf{V}$;
2. Compute $36N_xN_y$ algebraic matrix-vector multiplications of order N_z to obtain vector $\tilde{\mathbf{V}}$;
3. Compute $3N_z$ backward FFT of vector $\tilde{\mathbf{V}}$.

The multiplications in Step 2 are further divided into $4N_xN_y$ groups which are mutually data independent. This allows to implement the special scheme of distributed data storage and a parallel algorithm of IE solver, described below.

For simplicity, consider $2N_y$ nodes and assume that N_x is even. The distributed storage of matrix is organized in a special way: the half of block-vector $\widetilde{Q}(n,j)$, $j = 0\ldots N_x/2-1$ is stored at nth node, $n = 0\ldots N_y-1$, while $\widetilde{Q}(n,j)$, $j = N_x/2\ldots N_x$ is stored at node $n+N_y$, $n = 0\ldots N_y-1$, Table 1.

Node 0	...	Node N_y-1	Node N_y	...	Node $2N_y-1$
$\widetilde{Q}(0,0)$	...	$\widetilde{Q}(N_y-1,0)$	$\widetilde{Q}(0,N_x/2)$	...	$\widetilde{Q}(N_y-1,N_x/2)$
$\widetilde{Q}(0,1)$	...	$\widetilde{Q}(N_y-1,1)$	$\widetilde{Q}(0,N_x/2+1)$	...	$\widetilde{Q}(N_y-1,N_x/2+1)$
$\vdots$	...	$\vdots$	$\vdots$	...	$\vdots$
$\widetilde{Q}(0,N_x/2-1)$	...	$\widetilde{Q}(N_y-1,N_x-1)$	$\widetilde{Q}(0,N_x-1)$	...	$\widetilde{Q}(N_y-1,N_x-1)$

Table 1: Matrix storage organization

This storage organization is used to develop the solver with suitable features of parallelization:

(i) The coefficients of matrices B, S, R_1, R_2 stored at different nodes are computed simultaneously and completely data independent;
(ii) The iterative method is executed using the authors' distributed implementation of FGMRES Saad (1993), inspired by Fraysse et al (2003);
(iii) The distributed two-dimensional Fourier transform is computed via the authors' implementation using FFTW3 library Frigo and Johnson (2005) for local FFT;
(iv) The calculation of the local algebraic matrix-vector multiplication is processed by using OpenBLAS library Wang et al (2013) ;
(v) For all the stages of the computational process the hybrid MPI+OpenMP scheme is used.

To demonstrate the scalability of the implemented parallelization the COMMEMI3D-3 model is used with $N_x = 176$, $N_y = 224$, $N_z = 118$, that is with cubic subdomains with 25 m edges, Sect. 4. The computational experiments performed at "Bluegene/P", HPC "Lomonosov" (MSU) and Piz Daint (Swiss National Supercomputing Center) showed good speed increment depending on the number of processes (Fig. 2). Matrix calculation time includes time of FFT calculation of $\widehat{B}_n^m$. The solid black line means ideal linear speed up. Note, that for such high-contrast model matrix calculation time (crosses) is small enough compared to solving of the system of linear equations (circles). One can see that the scalability is close to a linear.

4 High Conductivity Contrast Modeling

The accurate computation of the EM field in a high conductivity contrast media is one of the most complex problems of EM modeling due to strong codependency between conductivity contrast and matrix condition number, Pankratov et al (1995); Pankratov and Kuvshinov (2016); Singer (1995). The conductivity contrast means the ratio between the real parts of anomalous conductivity $\mathbf{Re}\,\sigma_a(M)$ and background conductivity $\mathbf{Re}\,\sigma_b(M)$ at the same point M.

The high conductivity contrast COMMEMI3D-3 model, Hursan and Zhdanov (2002); Varentsov et al (2000), is used as one of the test models for the presented solver. This model schematically describes the conductivity distribution typical for

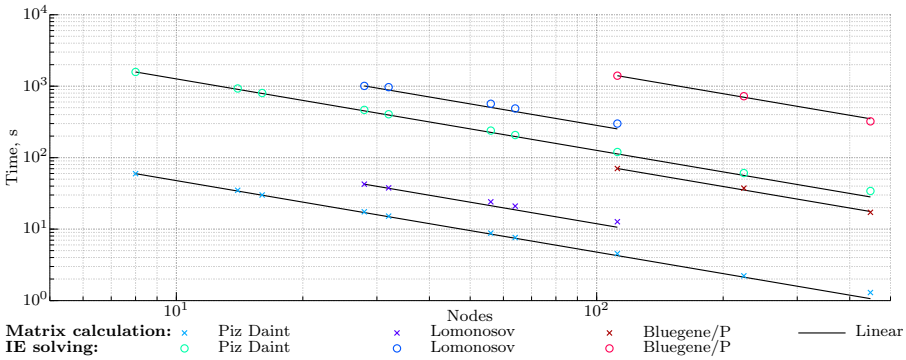

Fig. 2: Strong scalability for COMMEMI3D-3 model

	x_1	y_1	z_1	x_2	y_2	z_2	σ
1	0	2.4	0.05	3	2.8	0.3	0.0033
2	0	1.8	0.05	3	2.4	0.45	0.033
3	0	1.4	0.05	3	1.8	0.30	0.1
4	0	0.8	0.05	3	1.4	0.45	0.033
5	0	0.4	0.05	3	0.8	0.30	0.0033
6	3.4	2.8	0.2	4.4	4.8	1	10
7	1.4	0	1	2.4	5.6	3	3.3333

Table 2: The coordinates of the opposite corners (x_1, y_1, z_1), (x_2, y_2, z_2) in km and conductivities σ (S/m) of COMMEMI3D-3 blocks

the ore exploration by the audio-magnetotelluric sounding. Following magnetotelluric (i.e., low-frequency) sounding tradition in the rest of this section the conductivity is a real-valued function.

The COMMEMI3D-3 model consists of seven rectangular blocks placed in a layered media and oriented along coordinate axes. Their conductivities σ (in S/m) and positions (coordinates of the opposite corners in km) are listed in Table 2 and depicted in Fig. 3. The layered background of the model consists of the upper halfspace $z < 0$ (air) with conductivity of 0 S/m, two layers with the conductivity of 10^{-3}, 10^{-4} S/m, and a lower halfspace with conductvity of 0.1 S/m. The thickness of the first and the second layers is 1 and 6.5 km respectively. One can see that maximum conductivity contrast is 10^4 in the first layer and $3.3 \cdot 10^4$ in the second one.

The modeling of magnetotelluric sounding was performed for various discretizations (cubic subdomains of different sizes) and periods $T = 2\pi/\omega$, and was compared with the results from modern FE solver by Grayver and Kolev (2015). Figures 4 and 5 represent, correspondingly, the apparent resistivities ρ_{xy} at profile $x = 1.9$ km and ρ_{yx} at profile $y = 3.83$ km for the period 1 s. One can see that the agreement with FE (magenta circles) is good even for rather coarse anomaly discretization (black curve). The exception is the area $[3.5, 4.5]$ km on the profile $y = 3.83$ km (Fig. 5) above the high-conductivity block. This is amended by taking finer discretization (azure curve).

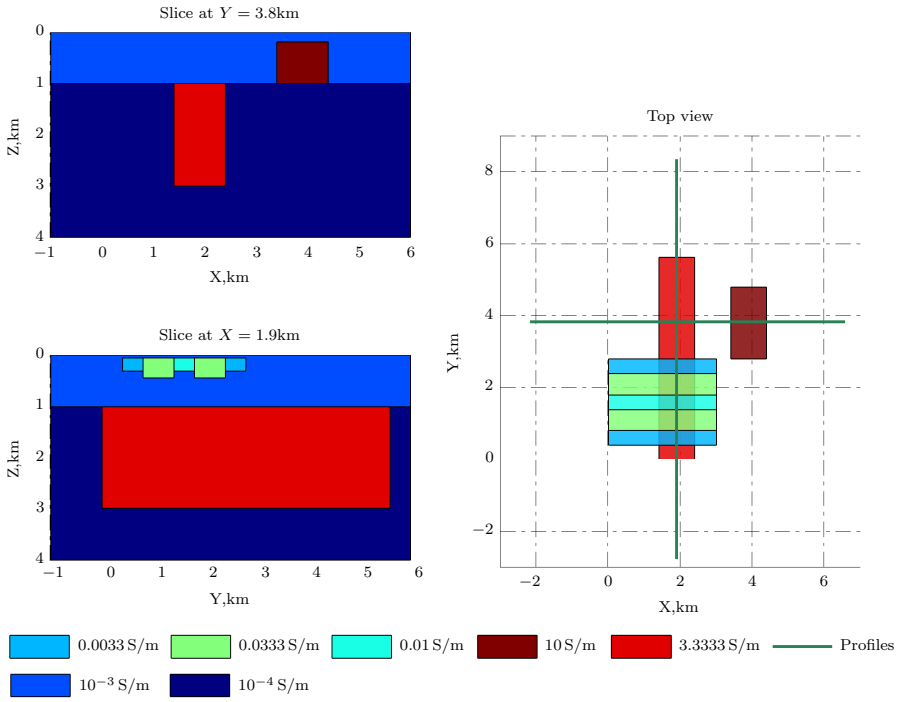

Fig. 3: Model COMMEMI3D-3

Figure 6 shows the apparent conductivity ρ_{yx} at site $(3.975, 3.83)$ km, that is above the high-conductivity block, at different periods. One can see that the finer discretization is needed only for the periods $\left[10^{-1}, 10^{1}\right]$ s. The reason behind this effect is the drastic change in the electric field inside of the compact high-conductivity block that does not allow to use the piecewise approximation on coarse discretization. The solver by Grayver and Kolev (2015) uses the second order polynomials which are very effective in such situations. At the same time, the coarse discretization can be efficiently used for smaller and larger periods. It is worth emphasizing that this concerns only the area above the high-conductivity block, while at the point $(1.9, 1.7)$ km, Fig. 7 shows good correspondence for all periods.

Figures 8 to 11 demonstrate area distribution of the apparent conductivity and impedance phases for 1 s period. One can see that the variation in apparent conductivity is of the four order of magnitude with very drastic transition. The phase change of the impedance is 10 degrees, and the transition is again drastic. It is worth reminding, that one of the peculiarities of IE method is quite weak dependence of computational costs on the number of sites where the field is computed. This allowed to obtain the maps with such drastic transitions without the additional computational costs.

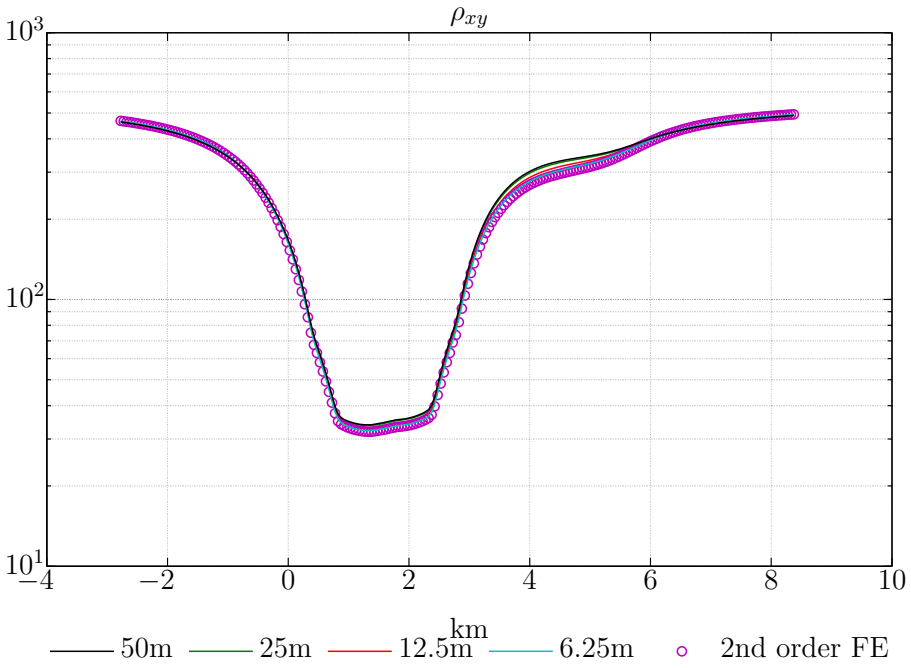

Fig. 4: Apparent resistivity ρ_{xy} at period 1 s along profile $x = 1.9$ km for different subdomain sizes

5 Conclusion

The presented solver named "Gnu Integral Equation Modeling in ElectroMagnetic Geophysics" (GIEM2G) shows impressive performance in terms of both memory requirements and accuracy. The memory requirements are 8 times lower compared to other volumetric IE solvers Avdeev et al (1997), Hursan and Zhdanov (2002). It is achieved for any layered background and non uniform discretization in vertical direction. In this way the average-scale modeling (up to $3 \cdot 10^6$ subdomains) can be efficiently done using laptops. The parallelization scheme allows to use HPC with hundreds and thousands of nodes for large-scale modeling (up to 10^9 subdomains).

The computational efficiency of the method is demonstrated on high-conductive contrast ($3.3 \cdot 10^4$) model COMMEMI3D-3. To the best of the authors knowledge, it is the first time that such high-contrast complex model provides comparable results for such different methods as FE and IE. In addition to the efficient usage of HPC the proposed IE method relies on the new technique to calculate the matrix coefficients. It is based on the analytical integration in vertical direction and completely new scheme to compute the integrals in horizontal direction. It is worth mentioning that the proposed scheme of analytical integration is robust in terms of machine precision and needs only $O(N_z)$ computations of complex exponents.

GIEM2G is implemented as hybrid MPI+OpenMP software on modern Fortran language. It is an open source software distributed under the GPLv2 license and can

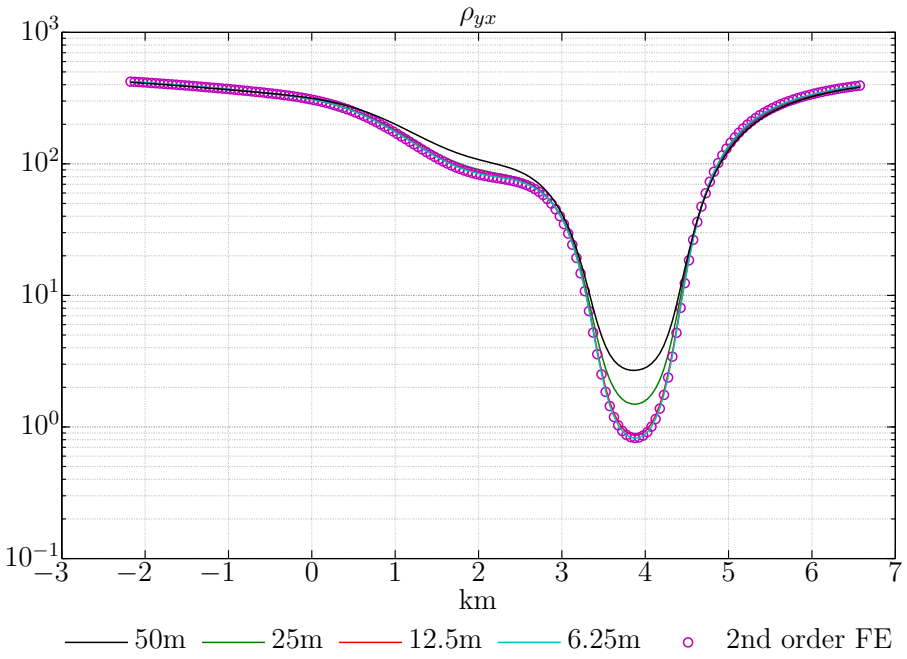

Fig. 5: Apparent resistivity ρ_{yx} at period 1 s along profile $y = 3.83$ km for different subdomain sizes

be simple cloned from GitLab by *git -clone git@gitlab.com:m.kruglyakov/GIEM2G.git*. It is also used as an optional computational engine in forward solver extrEMe Kruglyakov et al (2016a) and inverse solver extrEMe-I Kruglyakov et al (2016b).

Acknowledgements The research of the first author was supported by the Russian Foundation for Basic Research (grant no. 13-05-12018-OFI_M). As a visiting fellow in ETH Zurich he was also partially supported by the Swiss National Science Foundation (grant no. IZK0Z2_163494) and ETH Zurich. Authors acknowledge the teams of HPC CMC Lomonosov MSU for the access to "Bluegene/P" HPC, the Lomonosov MSU Research Computing Center for the access to HPC "Lomonosov" Sadovnichy et al (2013) and the Swiss National Supercomputing Center (CSCS) grant (project ID s577). Authors also would like to thank Alexander Grayver, ETH Zurich, for providing data for comparison and Alexey Kuvshinov, ETH Zurich, for suggestions and helpful discussions.

References

Anderson W (1979) Numerical integration of related hankel transforms of order 0 and 1 by adaptive digital filtering. Geophysics 44:1287–1305

Avdeev D, Knizhnik S (2009) 3D integral equation modeling with a linear dependence on dimensions. Geophysics 74:89–94

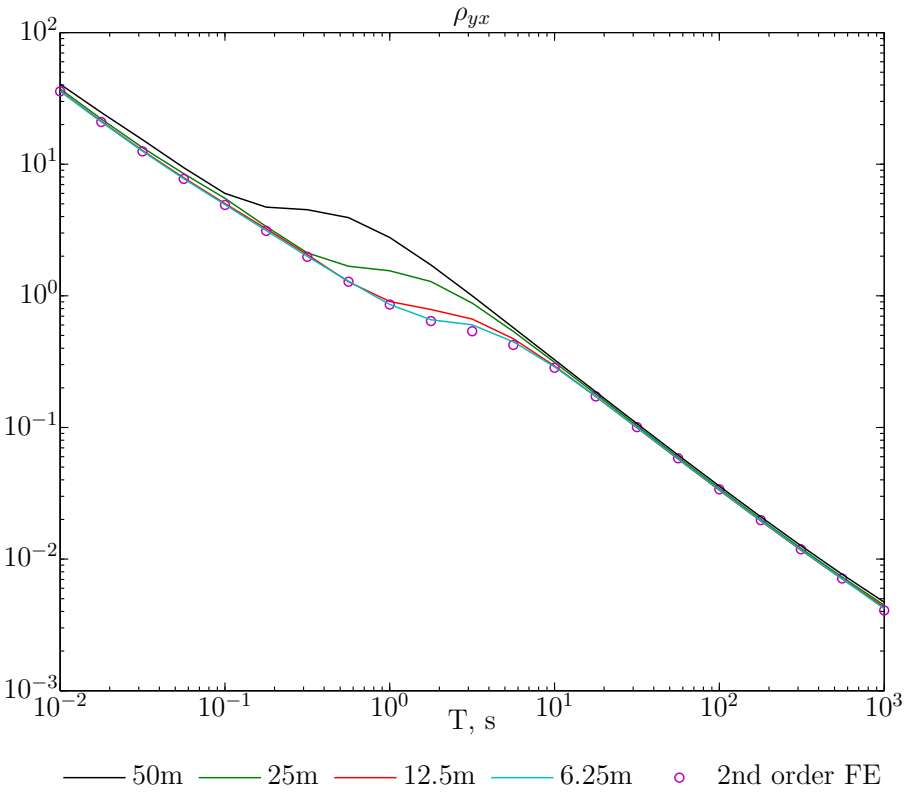

Fig. 6: Apparent resistivity ρ_{yx} at site $x = 3.975$ km, $y = 3.83$ km depends on period

Avdeev D, Kuvshinov A, Pankratov O, Newman G (2002) Three-dimensional induction logging problems, Part I: An integral equation solution and model comparisons. Geophysics 67(2):413–426

Avdeev DB, Kuvshinov AV, Pankratov OV, Newman GA (1997) High-performance three-dimensional electromagnetic modelling using modified Neumann series. Wide-band numerical solution and examples. J Geomagn Geoelectr 49:1519–1539

Chave A, Jones A (2012) The Magnetotelluric Method: Theory and Practice. Cambridge Univ. Press

Delves LM, Mohamed JL (1985) Computational Methods for Integral Equations. Cambridge University Press

Dmitriev V, Silkin A, Farzan R (2002) Tensor Green function for the system of Maxwell's equations in a layered medium. Comput Math and Modeling 13(2):107–118

Egbert GD, Kelbert A (2012) Computational recipes for electromagnetic inverse problems. Geophys J Int 189(1):251–267, DOI {10.1111/j.1365-246X.2011.05347.x}

Ernst O, Gander M (2012) Why it is difficult to solve helmholtz problems with classical iterative methods. In: Graham IG, Hou TY, Lakkis O, Scheichl R (eds) Nu-

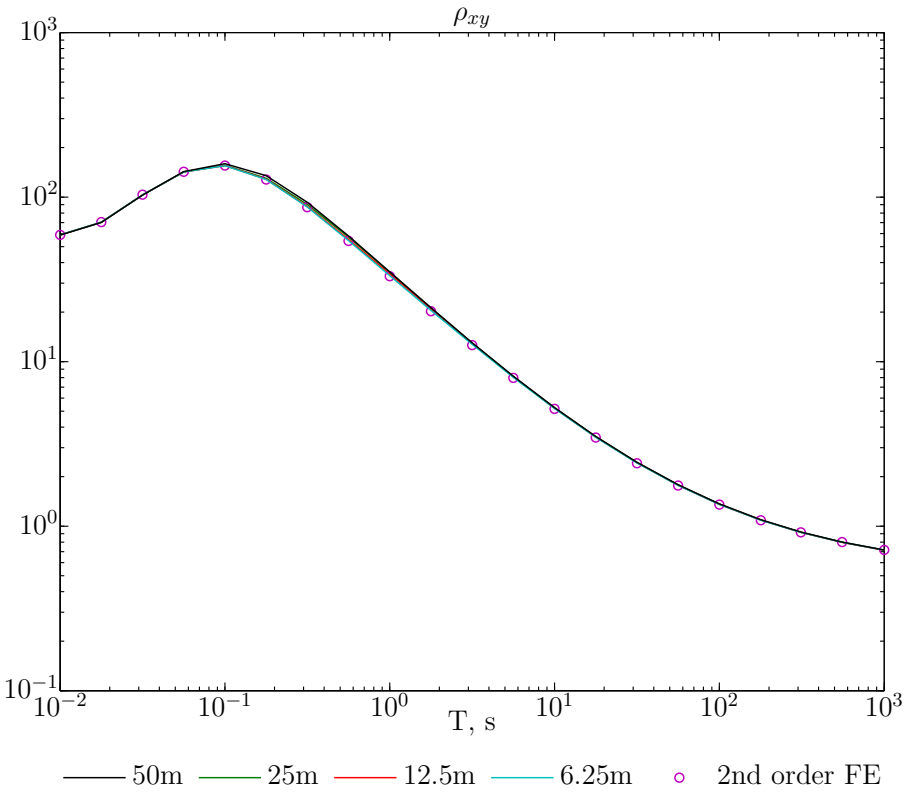

Fig. 7: Apparent resistivity ρ_{xy} at site $x = 1.9$ km, $y = 1.7$ km depends on period

merical Analysis of Multiscale Problems, Lecture Notes in Computational Science and Engineering, vol 83, Springer Berlin Heidelberg, pp 325–363

Farquharson CG, Miensopust MP (2011) Three-dimensional finite-element modelling of magnetotelluric data with a divergence correction. Journal of Applied Geophysics 75:699–710

Fraysse V, Giraud L, Gratton S, Langou J (2003) A set of GMRES routines for real and complex arithmetics on high performance computers. URL http://www.cerfacs.fr/algor/reports/2003/TR_PA_03_03.pdf

Frigo M, Johnson SG (2005) The design and implementation of FFTW3. Proceedings of the IEEE 93(2):216–231, special issue on "Program Generation, Optimization, and Platform Adaptation"

Grayver A, Kolev T (2015) Large-scale 3d geo-electromagnetic modeling using parallel adaptive high-order finite element method. Geophysics 80(6):277–291

Haber E, Ascher UM (2001) Fast finite volume simulation of 3D electromagnetic problems with highly discontinuous coefficients. SIAM Journal of Scientific Computing 22(6):1943–1961

Hursan G, Zhdanov MS (2002) Contraction integral equation method in three-dimensional electromagnetic modeling. Radio Science 37(6):1–1–1–

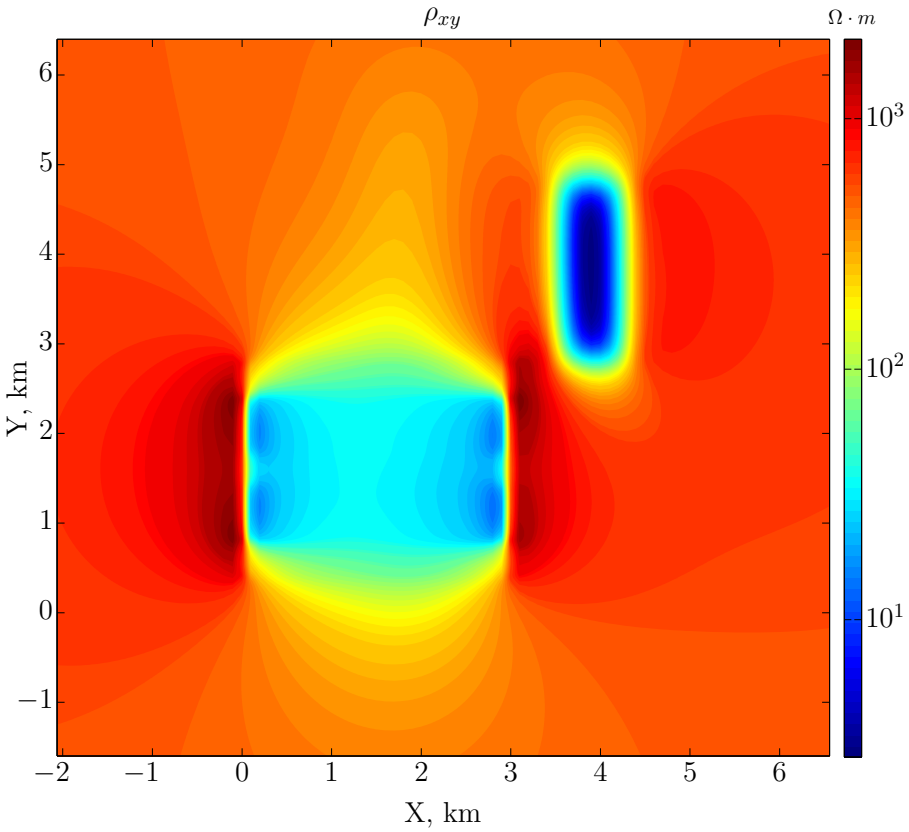

Fig. 8: Apparent resistivity ρ_{xy} at 1 s

13, DOI 10.1029/2001RS002513, URL http://dx.doi.org/10.1029/2001RS002513, 1089

Jaysaval P, Shantsev DV, de la Kethulle de Ryhove S (2015) Efficient 3-d controlled-source electromagnetic modelling using an exponential finite-difference method. Geophysical Journal International 203(3):1541–1574, DOI 10.1093/{Geophys.J. Int.}/ggv377

Kamm J, Pedersen LB (2014) Inversion of airborne tensor vlf data using integral equations. Geophysical Journal International 198(2):775–794, DOI 10.1093/{Geophys.J.Int.}/ggu161

Koyama T, Utada H, Avdeev D (2008) Fast and memory-saved 3-D forward modeling code for MT by using integral equation method. In: Abstract book, 19th workshop on electromagnetic induction in the Earth, China

Kruglyakov M (2011) Modified integral current methods in electrodynamics of non-homogeneous media. Comput Math and Modeling 22(3):246–254

Kruglyakov M, Geraskin A, Kuvshinov A (2016a) Novel accurate and scalable 3-d MT forward solver based on a contracting integral equation method. Com-

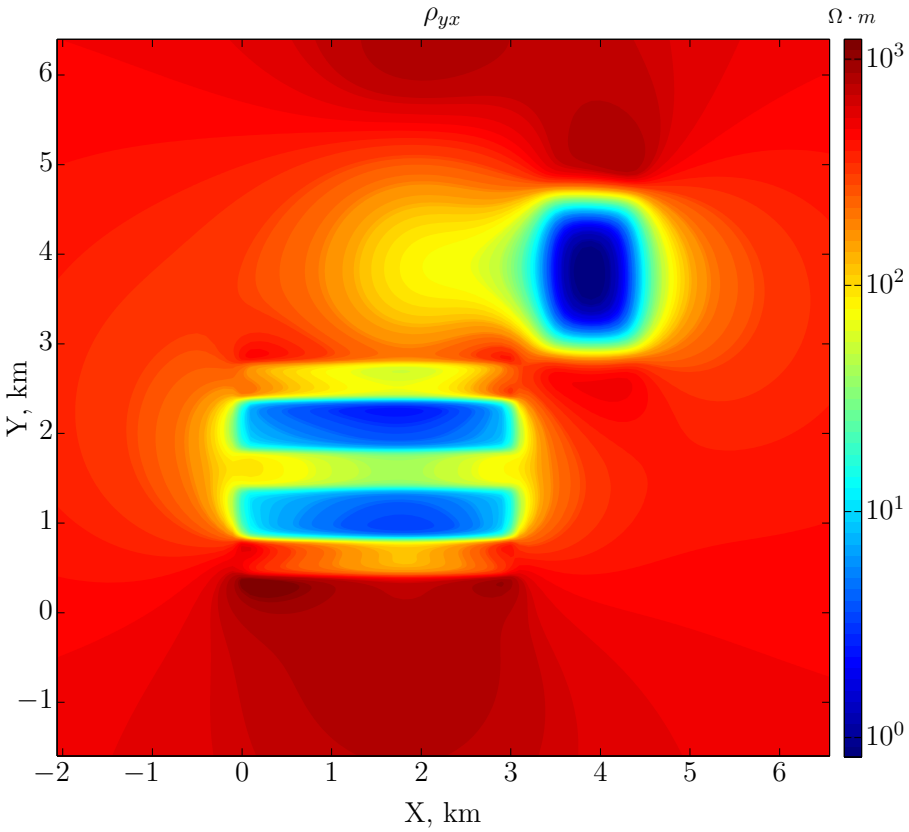

Fig. 9: Apparent resistivity ρ_{yx} at 1 s

puters & Geosciences 96:208 – 217, DOI http://dx.doi.org/10.1016/j.cageo.2016.08.017, URL http://www.sciencedirect.com/science/article/pii/S009830041630293X

Kruglyakov M, Geraskin A, Kuvshinov A (2016b) Novel Scalable 3-d MT Inverse Solver (extrEMe–I). In: Abstract GP51A-1357 presented at 2016 Fall Meeting, AGU, San Francisco, Calif. 12–16 Dec., AGU, San Francisco

Mackie R, Smith J, Madden T (1994) 3-Dimensional electromagnetic modeling using finite-difference equation – The magnetotelluric example. Radio Science 29(4):923–935

Mulder W (2006) A multigrid solver for 3D electromagnetic diffusion. Geophys Prospect 54:633–649

Newman G, Alumbaugh D (2002) Three-dimensional induction logging problems, Part 2: A finite-difference solution. Geophysics 61:484–491

Pankratov O, Kuvshinov A (2016) Applied mathematics in EM studies with special emphasis on an uncertainty quantification and 3-d integral equation modelling. Surveys in Geophysics 37(1):109–147, DOI 10.1007/s10712-015-9340-4, URL

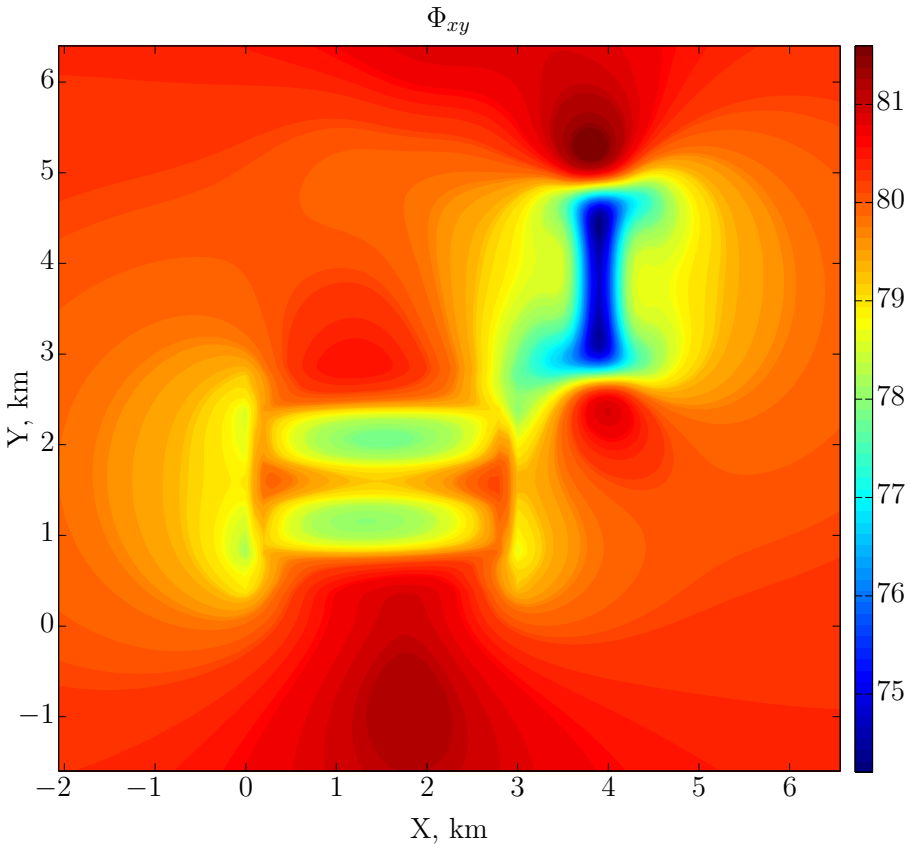

Fig. 10: Impedance phase Φ_{xy} at 1 s

http://dx.doi.org/10.1007/s10712-015-9340-4

Pankratov O, Avdeyev D, Kuvshinov A (1995) Electromagnetic-field scattering in a heterogeneous Earth: A solution to the forward problem. Izv-Phys Solid Eart+ 31(3):201–209

Puzyrev V, Koldan J, de la Puente J, Houzeaux G, Vazquez M, Cela JM (2013) A parallel finite-element method for three-dimensional controlled-source electromagnetic forward modelling. Geophys J Int 193:678–693

Raiche AP (1974) An integral equation approach to three-dimensional modelling. Geophys J Int 36(2):363–376

Ren Z, Kalscheuer T, Greenhalgh H S Maurer (2013) A goal-oriented adaptive finite-element approach for plane wave 3-D electromagnetic modelling. Geophys J Int 194:700–718

Saad Y (1993) A flexible inner-outer preconditioned GMRES algorithm. SIAM J Sci Comput 14(2):461–469

Sadovnichy V, Tikhonravov A, Voevodin V, Opanasenko V (2013) "Lomonosov": Supercomputing at Moscow State University. In: Contemporary High Performance

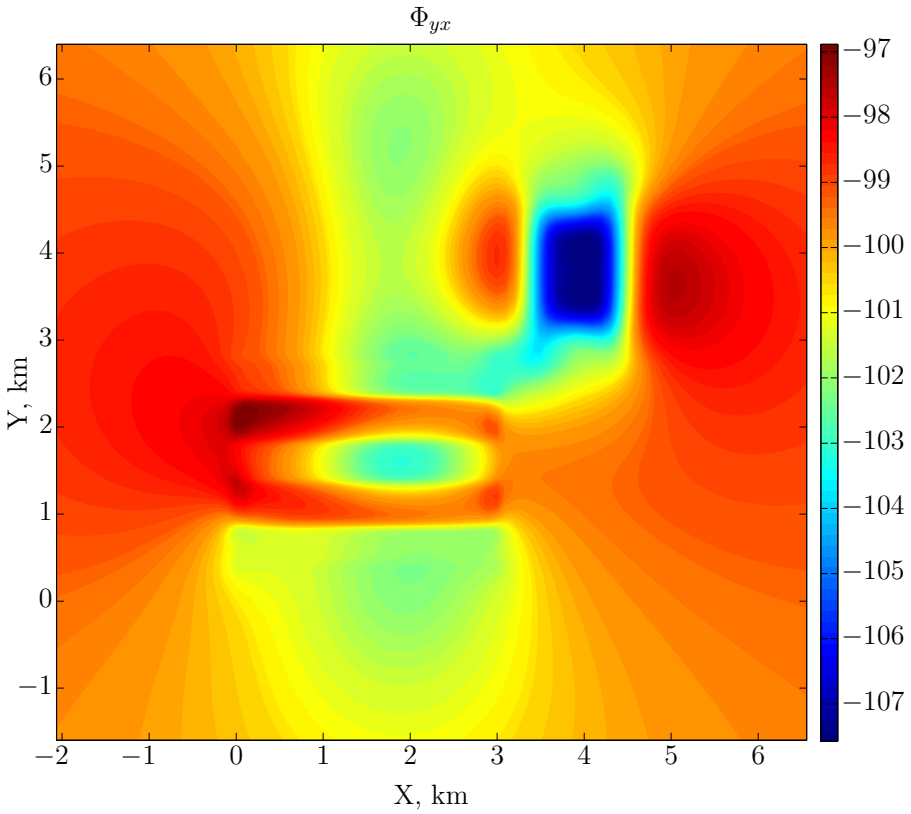

Fig. 11: Impedance phase Φ_{yx} at 1 s

Computing: From Petascale toward Exascale, Boca Raton, United States, Chapman & Hall/CRC Computational Science, pp 283–307

Schwarzbach C, Börner RU, Spitzer K (2011) Three-dimensional adaptive higher order finite element simulation for geo-electromagnetics - a marine CSEM example. Geophys J Int 187:63–74

Singer B (1995) Method for solution of Maxwell's equations in non-uniform media. Geophys J Int 120:590–598

Singer B (2008) Electromagnetic integral equation approach based on contraction operator and solution optimization in Krylov subspace. Geophys J Int 175:857–884

Sun J, Kuvshinov A (2015) Accelerating EM integral equation forward solver for global geomagnetic induction using SVD based matrix compression method. Geophys J Int 200(2):1005–1011

Varentsov IM, Fomenko IY, Golubev NG, Mehanee S, Hursan G, Zhdanov MS (2000) Comparative study of 3-D finite difference and integral equation methods. In: Proceedings of 2000 Consortium for Electomagnetic Modeling and Inversion Annual Meeting, University of Utah, Salt Lake City, pp 35–74

Wang Q, Zhang X, Zhang Y, Yi Q (2013) AUGEM: automatically generate high performance dense linear algebra kernels on x86 cpus. In: International Conference for High Performance Computing, Networking, Storage and Analysis, SC'13, Denver, CO, USA - November 17 - 21, 2013, pp 1–12, URL http://www.openblas.net.

Wannmaker PE (1991) Advances in three-dimensional magnetotelluric modeling using integral equations. Geophysics 56:1716–1728

Ward SH, Hohmann GW (1988) 4. Electromagnetic Theory for Geophysical Applications, SEG,USA, chap 4, pp 130–311

Weidelt P (1975) Electromagnetic induction in three-dimensional structures. J Geophys-Z Geophys 41:85–109

Appendix A: Green's Tensor

Following the notations from Dmitriev et al (2002), the electrical $\widehat{G}^E$ and magnetic $\widehat{G}^H$ tensors of layered media can be written as

$$\begin{aligned}\widehat{G}^E &= \widehat{G} + \operatorname{grad}\left(\frac{\mu_0}{k^2}\operatorname{div}\frac{\widehat{G}}{\mu_0}\right),\\ \widehat{G}^H &= \frac{1}{i\omega\mu_0}\operatorname{curl}\widehat{G},\\ k^2 &= i\omega\mu_0\sigma_b,\end{aligned} \tag{21}$$

where

$$\widehat{G}(M,M_0) = \begin{pmatrix} G_1(M,M_0) & 0 & 0\\ 0 & G_1(M,M_0) & 0\\ \frac{\partial g(M,M_0)}{\partial x} & \frac{\partial g(M,M_0)}{\partial y} & G_2(M,M_0)\end{pmatrix} \tag{22}$$

and

$$\begin{aligned} G_1(M,M_0) &= \frac{i\omega\mu_0}{4\pi}\int_0^\infty J_0(\lambda\rho)U_1(\lambda,z,z_0)\lambda d\lambda,\\ G_2(M,M_0) &= \frac{i\omega\mu_0}{4\pi}\int_0^\infty J_0(\lambda\rho)U_\sigma(\lambda,z,z_0)\lambda d\lambda,\\ g(M,M_0) &= -\frac{i\omega\mu_0}{4\pi}\int_0^\infty J_0(\lambda\rho)\left(\frac{\partial}{\partial z_0}U_\sigma(\lambda,z,z_0)+\frac{\partial}{\partial z}U_1(\lambda,z,z_0)\right)\frac{d\lambda}{\lambda},\\ M &= M(x,y,z)\quad M_0 = M_0(x_0,y_0,z_0)\quad \rho = \sqrt{(x-x_0)^2+(y-y_0)^2}.\end{aligned} \tag{23}$$

Here J_0 is a zero-order Bessel function of the first kind, and functions $U_\gamma(\lambda,z,z_0)$, $\gamma = 1,\sigma$ are the fundamental functions of the layered media (Appendix B).

From (21) and (22) one gets

$$\widehat{G}^E = \begin{Bmatrix} G_1 + \frac{1}{k^2}\frac{\partial^2}{\partial x^2}\left(G_1 + \frac{\partial g}{\partial z}\right) & \frac{1}{k^2}\frac{\partial^2}{\partial x \partial y}\left(G_1 + \frac{\partial g}{\partial z}\right) & \frac{1}{k^2}\frac{\partial^2 G_2}{\partial x \partial z} \\ \frac{1}{k^2}\frac{\partial^2}{\partial x \partial y}\left(G_1 + \frac{\partial g}{\partial z}\right) & G_1 + \frac{1}{k^2}\frac{\partial^2}{\partial y^2}\left(G_1 + \frac{\partial g}{\partial z}\right) & \frac{1}{k^2}\frac{\partial^2 G_2}{\partial y \partial z} \\ \frac{\partial g}{\partial x} + \frac{1}{k^2}\frac{\partial^2}{\partial x \partial z}\left(G_1 + \frac{\partial g}{\partial z}\right) & \frac{\partial g}{\partial y} + \frac{1}{k^2}\frac{\partial^2}{\partial y \partial z}\left(G_1 + \frac{\partial g}{\partial z}\right) & G_2 + \frac{1}{k^2}\frac{\partial^2 G_2}{\partial z^2} \end{Bmatrix}. \tag{24}$$

Note, that $G^E_{xz}(M,M_0) = -G^E_{zx}(M_0,M)$, $G^E_{yz}(M,M_0) = -G^E_{zy}(M_0,M)$ according to Lorentz reciprocity.

Let $\Omega_n = S_n \times [z_n^1, z_n^2]$, $\Omega_m = S_m \times [z_m^1, z_m^2]$, where S_n, S_m are horizontal rectangular domains, and let $\sigma_b = \sigma_b^n$ inside $[z_n^1, z_n^2]$, $\sigma_b = \sigma_b^m$ inside $[z_m^1, z_m^2]$. That is the subdomains do not intersect the boundaries of the layers. Taking into account (12), (21) and (24) one can see that $\widehat{B}_n^m$ is expressed in terms of double volumetric integrals with weak integrable singularity, so the order of integration can be changed. Then using (23) and (24) one obtains

$$\widehat{B}_n^m = \frac{1}{4\pi}\begin{Bmatrix} I_1^{n,m} + I_{xx}^{n,m} & I_{xy}^{n,m} & I_x^{n,m} \\ I_{xy}^{n,m} & I_1^{n,m} + I_{yy}^{n,m} & I_y^{n,m} \\ -I_x^{m,n} & -I_y^{m,n} & I_2^{n,m} + I_{zz}^{n,m} \end{Bmatrix}, \tag{25}$$

where

$$\begin{aligned}
I_1^{n,m} &= \int_{S_n}\int_{S_m}\left(\int_0^\infty J_0(\lambda\rho)V_1^{n,m}(\lambda)\lambda d\lambda\right) dx_0 dy_0 dx dy, \\
I_2^{n,m} &= \int_{S_n}\int_{S_m}\left(\int_0^\infty J_0(\lambda\rho)V_2^{n,m}(\lambda)\lambda d\lambda\right) dx_0 dy_0 dx dy, \\
I_{\alpha\beta}^{n,m} &= \int_{S_n}\frac{\partial^2}{\partial\alpha\partial\beta}\left\{\int_{S_m}\left(\int_0^\infty J_0(\lambda\rho)\left[V_1^{n,m}(\lambda) + V_3^{n,m}(\lambda)\right]\frac{d\lambda}{\lambda}\right) dx_0 dy_0\right\} dx dy, \\
I_\alpha^{n,m} &= \int_{S_n}\frac{\partial}{\partial\alpha}\left\{\int_{S_m}\left(\int_0^\infty J_0(\lambda\rho)V_4^{n,m}(\lambda)\lambda d\lambda\right) dx_0 dy_0\right\} dx dy, \\
I_{zz}^{n,m} &= \int_{S_n}\int_{S_m}\left(\int_0^\infty J_0(\lambda\rho)V_5^{n,m}(\lambda)\lambda d\lambda\right) dx_0 dy_0 dx dy.
\end{aligned} \tag{26}$$

Here $\alpha = x, y$, $\beta = x, y$, and

$$V_1^{n,m}(\lambda) = i\omega\mu_0 \int_{z_n^1}^{z_n^2} \int_{z_m^1}^{z_m^2} U_1(\lambda, z, z_*) dz_* dz,$$

$$V_2^{n,m}(\lambda) = i\omega\mu_0 \int_{z_n^1}^{z_n^2} \int_{z_m^1}^{z_m^2} U_\sigma(\lambda, z, z_*) dz_* dz,$$

$$V_3^{n,m}(\lambda) = -\frac{1}{\sigma_b^n} \int_{z_n^1}^{z_n^2} \frac{\partial}{\partial z} \left(\int_{z_m^1}^{z_m^2} \left[\frac{\partial}{\partial z_*} U_\sigma(\lambda, z, z_*) \right] dz_* \right) dz,$$

$$V_4^{n,m}(\lambda) = \frac{1}{\sigma_b^n} \int_{z_n^1}^{z_n^2} \frac{\partial}{\partial z} \left(\int_{z_m^1}^{z_m^2} U_\sigma(\lambda, z, z_*) dz_* \right) dz,$$

$$V_5^{n,m}(\lambda) = \frac{1}{\sigma_b^n} \int_{z_n^1}^{z_n^2} \frac{\partial^2}{\partial z^2} \left(\int_{z_m^1}^{z_m^2} U_\sigma(\lambda, z, z_*) dz_* \right) dz. \tag{27}$$

Therefore, to obtain the coefficients of $\hat{B}_n^m$ one needs computational methods to find "horizontal" integrals (26) and "vertical" integrals (27). These methods are presented in the next sections.

Appendix B: Vertical Integration

The integrals in (27) are expressed in terms of the so-called fundamental function of the layered media, Dmitriev et al (2002). Consider the media with $N_{lay} - 1$ homogenous layers with complex conductivities σ_n, $n = 1 \ldots N_{lay} - 1$, the upper halfspace (air, the zeroth layer) with complex conductivity σ_0 and the lower halfspace (the N_{lay}-th layer) with conductivity $\sigma_{N_{lay}}$. Note, that in EM sounding problems typically $\mathbf{Re}\,\sigma_0 \leq 10^{-9}$.

The function $U_\gamma(z,z_*,\lambda)$ is defined as a unique solution of the problem

$$\begin{cases} \dfrac{\partial^2}{\partial z^2}U_\gamma(z,z_*,\lambda)-\eta_0^2U_\gamma(z,z_*,\lambda)=0, z<d_1, z\neq z_*,\\ \dfrac{\partial^2}{\partial z^2}U_\gamma(z,z_*,\lambda)-\eta_n^2U_\gamma(z,z_*,\lambda)=0, d_n<z<d_{n+1}, z\neq z_*,\\ \dfrac{\partial^2}{\partial z^2}U_\gamma(z,z_*,\lambda)-\eta_{N_{lay}}^2U_\gamma(z,z_*,\lambda)=0, z>d_{N_{lay}}, z\neq z_*,\\ \left[U_\gamma(z,z_*,\lambda)\right]_{z=d_n}=0,\\ \left[\dfrac{1}{\gamma}\dfrac{\partial}{\partial z}U_\gamma(z,z_*,\lambda)\right]_{z=d_n}=0,\\ \left[U_\gamma(z,z_*,\lambda)\right]_{z=z_*}=0,\\ \left[\dfrac{\partial}{\partial z}U_\gamma(z,z_*,\lambda)\right]_{z=z_*}=-2,\\ \left|U_\gamma(z,z_*,\lambda)\right|\to 0 \text{ as } z\to\pm\infty,\\ \eta_m^2=\lambda^2-k_m^2,\quad k_m^2=i\omega\mu_0\sigma_m,\\ m=0\ldots N_{lay},\quad n=1\ldots N_{lay}-1,\quad 0<\lambda<\infty. \end{cases} \tag{28}$$

The following procedure is performed to obtain an explicit expression for U_γ that allows analytical integration. Let $l_0=0$, $l_{N_{lay}}=0$, $l_n=d_{n+1}-d_n$, $n=1\ldots N_{lay}-1$. Define p_m^γ, q_m^γ, $m=0\ldots N_{lay}$ by the recurrent expressions

$$\begin{aligned} &p_0^\gamma=0; && q_{N_{lay}}^\gamma=0;\\ &p_1^\gamma=\frac{1-\alpha_0^\gamma\frac{\eta_0}{\eta_1}}{1+\alpha_0^\gamma\frac{\eta_0}{\eta_1}}; && q_{N_{lay}-1}^\gamma=\frac{1-\beta_{N_{lay}}^\gamma\frac{\eta_{N_{lay}}}{\eta_{N_{lay}-1}}}{1+\beta_{N_{lay}}^\gamma\frac{\eta_{N_{lay}}}{\eta_{N_{lay}-1}}};\\ &p_{m+1}^\gamma=\frac{1+\alpha_m^\gamma\frac{\eta_m}{\eta_{m+1}}\frac{p_m^\gamma e^{-2\eta_m l_m}-1}{p_m^\gamma e^{-2\eta_m l_m}+1}}{1-\alpha_m^\gamma\frac{\eta_m}{\eta_{m+1}}\frac{p_m^\gamma e^{-2\eta_m l_m}-1}{p_m^\gamma e^{-2\eta_m l_m}+1}}, && q_{m-1}^\gamma=\frac{1+\beta_m^\gamma\frac{\eta_m}{\eta_{m-1}}\frac{q_m^\gamma e^{-2\eta_m l_m}-1}{q_m^\gamma e^{-2\eta_m l_m}+1}}{1-\beta_m^\gamma\frac{\eta_m}{\eta_{m-1}}\frac{q_m^\gamma e^{-2\eta_m l_m}-1}{q_m^\gamma e^{-2\eta_m l_m}+1}},\\ &\quad m\neq N_{lay}; && \quad m\neq 0;\\ &\alpha_m^\gamma=\begin{cases}1,\gamma=1;\\ \dfrac{\sigma_{m+1}}{\sigma_m},\gamma=\sigma;\end{cases} && \beta_m^\gamma=\begin{cases}1,\gamma=1;\\ \dfrac{\sigma_{m-1}}{\sigma_m},\gamma=\sigma.\end{cases} \end{aligned} \tag{29}$$

Let $d_0=d_1$, $d_{N_{lay+1}}=d_{N_{lay}}$ and let points z_r, z_s belong to r and s layers respectively, $0\le r,s\le N_{lay}$. Then using (29) one gets

$$U_\gamma(z_r,z_s,\lambda)=\begin{cases} A_{r,s}^\gamma\left(p_r^\gamma e^{2\eta_r d_r}e^{-\eta_r z_r}+e^{\eta_r z_r}\right)\left(e^{-\eta_s z_s}+q_s^\gamma e^{-2\eta_s d_{s+1}}e^{\eta_s z_s}\right)\\ \qquad\qquad \text{for}\quad z_r\le z_s;\\ A_{s,r}^\gamma\left(p_s^\gamma e^{2\eta_s d_s}e^{-\eta_s z_s}+e^{\eta_s z_s}\right)\left(e^{-\eta_r z_r}+q_r^\gamma e^{-2\eta_r d_{r+1}}e^{\eta_r z_r}\right)\\ \qquad\qquad \text{for}\quad z_r>z_s, \end{cases} \tag{30}$$

where

$$
\begin{aligned}
A^{\gamma}_{r,s} &= Q^{\gamma}_{r} \times Q^{\gamma}_{r+1} \times \cdots \times Q^{\gamma}_{s-1} A^{\gamma}_{s,s}, \quad \text{for} \quad r < s, \\
Q^{\gamma}_{m} &= \frac{1 + p^{\gamma}_{m+1}}{1 + p^{\gamma}_{m} e^{-2\eta_m l_m}} e^{(\eta_{m+1} - \eta_m) d_{m+1}}, \quad \text{for} \quad m = 1 \ldots N_{lay} - 1, \\
A^{\gamma}_{n,n} &= \frac{1}{\eta_n \left(1 - p^{\gamma}_{n} q^{\gamma}_{n} e^{-2\eta_n l_n}\right)}, \quad \text{for} \quad r = s = n, n = 0 \ldots N_{lay}, \\
A^{1}_{r,s} &= A^{1}_{s,r}, \quad A^{\sigma}_{r,s} = \frac{\sigma_r}{\sigma_s} A^{\sigma}_{s,r}, \quad \text{for} \quad r > s.
\end{aligned}
\tag{31}
$$

To check (30) one can explicitly substitute (30) in (28) taking into account (29) and (31).

In view of (30) one can see that integrals in (27) (i.e., the integrals over $U_{\gamma}(z, z_*, \lambda)$ and its partial derivatives) can be integrated analytically with respect to z, z_* over any domains that do not intersect the layer boundaries. However, the rounding errors arising in addition and multiplication of very small or large quantities make the formula (30) impractical for $\lambda \gg 1$. Instead the following formula is used

$$
U_{\gamma}(z_r, z_s, \lambda) = \begin{cases}
A^{\gamma}_{r,s} \Big(p^{\gamma}_{r} e^{-(\eta_r z_r + \eta_s z_s - 2\eta_r d_r)} + q^{\gamma}_{s} e^{-(2\eta_s d_{s+1} - (\eta_r z_r + \eta_s z_s))} + \\
\qquad e^{-(\eta_s z_s - \eta_r z_r)} + p^{\gamma}_{r} q^{\gamma}_{s} e^{-(2(\eta_s d_{s+1} - \eta_r d_r) - (\eta_s z_s - \eta_r z_r))} \Big) \\
\qquad\qquad \text{for} \quad z_r \le z_s; \\
A^{\gamma}_{s,r} \Big(p^{\gamma}_{s} e^{-(\eta_s z_s + \eta_r z_r - 2\eta_s d_s)} + q^{\gamma}_{r} e^{-(2\eta_r d_{r+1} - (\eta_s z_s + \eta_r z_r))} + \\
\qquad e^{-(\eta_r z_r - \eta_r z_r)} + p^{\gamma}_{s} q^{\gamma}_{r} e^{-(2(\eta_r d_{r+1} - \eta_s d_s) - (\eta_r z_r - \eta_s z_s))} \Big) \\
\qquad\qquad \text{for} \quad z_r > z_s.
\end{cases}
\tag{32}
$$

Formula (32) overcomes the aforementioned problem, since the real parts of all the exponents powers are negative. The consequent calculations provide accurate and robust results for any $0 < \lambda < \infty$.

Consider N_z subdomains in the discretization in vertical direction. To obtain the matrix $\widehat{B}^{m}_{n}$ for the system (15) one needs to compute $O\left(N_z^2\right)$ complex exponents in (32). An algorithm requiring only $O\left(N_z\right)$ complex exponents calculations is developed to speed up the integration procedure.

Let $z_0 < z_1 < \cdots < z_{N_z}$. Suppose that the intervals $[z_l, z_{l+1}]$, $l = 0 \ldots N_z - 1$ do not intersect the layers' boundaries. For $i, j = 0 \ldots N_z - 1$, $0 \le \alpha + \beta \le 2$ one needs to calculate $W^{\alpha,\beta}_{i,j}(\gamma) = \int\limits_{z_i}^{z_{i+1}} \frac{\partial^{\alpha}}{\partial z^{\alpha}} \left(\int\limits_{z_j}^{z_{j+1}} \left[\frac{\partial^{\beta}}{\partial z_*^{\beta}} U_{\gamma}(z, z_*, \lambda) \right] dz_* \right) dz$.

Let r_l be an index of the layer containing $[z_l, z_{l+1}]$, $l = 0 \ldots N_z - 1$. Then using (30) one obtains for $z_i < z_j$

$$
\begin{aligned}
W^{\alpha,\beta}_{i,j}(\gamma) = \int\limits_{z_i}^{z_{i+1}} \left(\frac{\partial^{\alpha}}{\partial z^{\alpha}} \int\limits_{z_j}^{z_{j+1}} \left[\frac{\partial^{\beta}}{\partial z_*^{\beta}} U_{\gamma}(z, z_*, \lambda) \right] dz_* \right) dz = \\
H^{\alpha}_{\gamma}(z_i, z_{i+1}) \prod_{l=i+1}^{l=j} \Theta^{\gamma}_{l} \int\limits_{z_j}^{z_{j+1}} \left(\frac{\partial^{\beta}}{\partial z_*^{\beta}} U\gamma(z_j, z_*, \lambda) \right) dz_*,
\end{aligned}
\tag{33}
$$

where

$$H_\gamma^\alpha(z_i,z_{i+1})=\frac{\int\limits_{z_i}^{z_{i+1}}\left(\frac{\partial^\alpha}{\partial z^\alpha}\left[p_{r_i}^\gamma e^{-\eta_{r_i}\left(z+z_{i+1}-2d_{r_i}\right)}+e^{-\eta_{r_i}(z_{i+1}-z)}\right]\right)dz}{p_{r_i}^\gamma e^{-2\eta_{r_i}\left(z_{i+1}-d_{r_i}\right)}+1},$$

$$\begin{aligned}\Theta_l^\gamma&=\varkappa_l^\gamma\frac{p_{r_l}^\gamma e^{-\eta_{r_l}\left((z_l+z_{l+1})-2d_{r_l}\right)}+e^{-\eta_{r_l}(z_{l+1}-z_l)}}{p_{r_l}^\gamma e^{2\eta_{r_l}(d_{r_l}-z_{l+1})}+1},\\ \varkappa_l^\gamma&=\left\{\begin{array}{c}1,r_l=r_{l+1}\\ Q_{r_{l+1}}^\gamma,r_l\neq r_{l+1}\end{array}\right\}.\end{aligned}\tag{34}$$

All the exponents in (34) vanish as $\lambda\to\infty$, so the corresponding computations do not depend on the round-off errors due to the machine precision. The formulas for $z_i>z_j$ are similar. The integrals $W_{ii}^{\alpha,\beta}$ are computed analytically using (32). Since Θ_l^γ depends only on $l=1\ldots N_z$ and $\gamma=1,\sigma$, one only needs to calculate $O(N_z)$ complex exponents using factorization (33), (34).

Appendix C: Horizontal Integration

The integrals (26) are the particular case of the integral

$$\begin{aligned}I_{\alpha,\beta}&=\int\limits_{S_n}\frac{\partial^{\alpha+\beta}}{\partial x^\alpha\partial y^\beta}\left\{\int\limits_{S_m}\left[\int\limits_0^\infty J_0(\rho\lambda)f(\lambda)d\lambda\right]dS_m\right\}dS_n,\\ \rho&=\sqrt{(x-x_0)^2+(y-y_0)^2},\quad 0\le\alpha+\beta\le 2,\end{aligned}\tag{35}$$

where $f(\lambda)$ is some easily computed function, $S_n=[x_n,x_n+h_x]\times[y_n,y_n+h_y]$, $S_m=[x_m,x_m+h_x]\times[y_m,y_m+h_y]$ are the rectangular domains with similar sizes.

The key feature of the proposed method is transformation of integrals (35) to one-dimensional convolution integral. Taking for simplicity $\alpha=\beta=0$, one has

$$I_{0,0}=F(R;p,q,\varphi)=\int\limits_0^\infty K(R\lambda;p,q,\varphi)f(\lambda)\frac{d\lambda}{\lambda^4},$$

$$\begin{aligned}K(R\lambda;p,q,\varphi)&=\lambda^4\int\limits_{S_m}\int\limits_{S_n}J_0(\rho\lambda)dS_mdS_n\\ &=\lambda^4\int\limits_{x_n}^{x_n+h_x}\int\limits_{y_n}^{y_n+h_y}\int\limits_{x_m}^{x_m+h_x}\int\limits_{y_m}^{y_m+h_y}J_0(\rho\lambda)dx_0dy_0dxdy\\ &=\int\limits_0^{R\lambda p}\int\limits_0^{R\lambda q}\int\limits_{R\lambda\left(\cos\varphi-\frac{p}{2}\right)}^{R\lambda\left(\cos\varphi+\frac{p}{2}\right)}\int\limits_{R\lambda\left(\sin\varphi-\frac{q}{2}\right)}^{R\lambda\left(\sin\varphi+\frac{q}{2}\right)}J_0(\tau)d\tilde{x}d\tilde{x}_0d\tilde{y}d\tilde{y}_0,\end{aligned}\tag{36}$$

where

$$\tau = \sqrt{(\tilde{x}-\tilde{x}_0)^2+(\tilde{y}-\tilde{y}_0)^2};$$
$$R = \sqrt{\left(x_n - x_m - \frac{h_x}{2}\right)^2 + \left(y_n - y_m - \frac{h_y}{2}\right)^2};$$
$$p = \frac{h_x}{R} \quad q = \frac{h_y}{R} \quad \varphi = \arctan\frac{y_n - y_m - \frac{h_y}{2}}{x_n - x_m - \frac{h_x}{2}}.$$

Let $\lambda = e^{-t}$, $R = e^s$

$$F\left(e^s; p, q, \varphi\right) = e^{3s}\int_{-\infty}^{\infty} \Phi(s-t; p, q, \varphi) f\left(e^{-t}\right) dt,$$
$$\Phi(s-t; p, q, \varphi) = K\left(e^{s-t}; p, q, \varphi\right) e^{-3(s-t)}. \tag{37}$$

For fixed p, q, φ the integral in (37) is the convolution integral with kernel Φ. Note that for different values of α and β the kernels can be obtained similarly.

The main advantage of using the convolution integrals is that their computation does not require the explicit calculation of kernel Φ. Consider the input function $v(t)$ and the output function $u(s)$ such that

$$u(s) = \int_{-\infty}^{+\infty} \Phi(s-t)v(t)dt. \tag{38}$$

For some $N = 2M$, l, $0 < \xi < 0.5l$, $k = -M \ldots M-1$, define

$$W_s = (-1)^s \frac{1}{N} \sum_{n=-M}^{M-1} \left\{ \frac{\sum_{m=-M}^{M-1} (-1)^m u(ml-\xi) e^{-2i\pi \frac{mn}{N}}}{\sum_{m=-M}^{M-1} (-1)^m v(ml+0.5l) e^{-2i\pi \frac{mn}{N}}} \right\} e^{2i\pi \frac{sn}{N}}. \tag{39}$$

Then for any $g(t)$ one gets

$$\int_{-\infty}^{+\infty} \Phi(s-t)g(t)dt \approx \sum_{s=N_1}^{N_2} W_s g(sl+\xi), \quad -M \le N_1 < N_2 \le M-1. \tag{40}$$

The tradeoff between the accuracy of (40) and the computational time is achieved by the particular selection of M, N_1, N_2, l, ξ and functions u and v.

From (36) and (40) the approximation formulas for (35) can be obtained

$$I_{\alpha,\beta} \approx R^{(3-\alpha-\beta)} \sum_{m=N_1}^{m=N_2} W_m^{\alpha,\beta}(p, q, \varphi, \alpha, \beta) f\left(\frac{\lambda_m}{R}\right),$$
$$\lambda_m = e^{ml+\xi}. \tag{41}$$

For the given input function $v(t) = 8e^{-t^2}\left(t^5 - 4t^3 + 2t\right)$ the output functions for different kernels can be expressed analytically by Gaussian and error functions. Inspired by Anderson (1979) the parameters used are $l = 0.2$, $\xi = 0.0964$, $M = 512$, $N_1 = -250$, $N_2 = 200$. In computational experiments these parameters provided appropriate accuracy in calculation of $\widehat{B}_n^m$.